ORIGINAL ARTICLE

Characterization of activated carbons for water treatment using TGA-FTIR for analysis of oxygen-containing functional groups

Daniel Dittmann[1,2] · Leon Saal[1,2] · Frederik Zietzschmann[3] · Maike Mai[4] · Korinna Altmann[2] · Dominik Al-Sabbagh[2] · Pia Schumann[1,4] · Aki Sebastian Ruhl[1,4] · Martin Jekel[4] · Ulrike Braun[1,2]

Abstract

Water treatment with activated carbon (AC) is an established method for the removal of organic micropollutants and natural organic matter. However, it is not yet possible to predict the removal of individual pollutants. An appropriate material characterization, matching adsorption processes in water, might be the missing piece in the puzzle. To this end, this study examined 25 different commercially available ACs to evaluate their material properties. Frequently reported analyses, including N_2 adsorption/desorption, CHNS(O), point of zero charge (PZC) analysis, and X-ray photoelectron spectroscopy, were conducted on a selected subset of powdered ACs. Inorganic elements examined using X-ray fluorescence and X-ray diffraction spectroscopy revealed that relative elemental contents were distinctive to the individual AC's raw material and activation procedure. This study also is the first to use thermogravimetric analysis (TGA) coupled to Fourier-transform infrared spectroscopy (FTIR) to conduct quantitative analyses of functional surface oxygen groups (SOGs: carboxylic acid, anhydride, lactone, phenol, carbonyl, and pyrone groups) on such a large number of ACs. The comparably economical TGA method was found to provide good surrogates for the PZC by pyrolytic mass loss up to 600 °C (ML_{600}), for the oxygen content by ML_{1000} and for the carbon content by oxidation. Mass loss profiles depict the AC's chemistry like fingerprints. Furthermore, we found that SOG contents determined by TGA-FTIR covered a wide individual range and depended on the raw material and production process of the AC. TGA and TGA-FTIR might therefore be used to identify the suitability of a particular AC for a variety of target substances in different target waters. This can help practitioners to control AC use in waterworks or wastewater treatment plants.

Keywords Adsorption · Organic contaminants · Proximate analysis · Thermogravimetry · Temperature-programmed desorption · Principal component analysis

Introduction

Adsorption onto activated carbon (AC) is a widespread process for the remediation of contaminated groundwater and soil, or for flue gas treatment (Worch 2021; Bandosz 2006).

✉ Daniel Dittmann
daniel.dittmann@uba.de

1 German Environment Agency (UBA), Schichauweg 58, 12307 Berlin, Germany

2 Bundesanstalt für Materialforschung und -prüfung, Unter den Eichen 87, 12205 Berlin, Germany

3 Berliner Wasserbetriebe, Motardstr. 35, 13629 Berlin, Germany

4 Technische Universität Berlin, Water Quality Control, Straße des 17. Juni 135, 10623 Berlin, Germany

Waterworks and municipal wastewater treatment plants apply ACs to cope with increasing concentrations of organic micropollutants (OMPs) in water cycles (Golovko et al. 2020; Rizzo et al. 2019; Guillossou et al. 2019). However, removal efficiencies in water are still not predictable today because of the large number of relatively complex interactions between the adsorbent, OMPs, and the water matrix (Kah et al. 2017; Moreno-Castilla 2004; Dittmar et al. 2018). In addition, the highly inconsistent material properties of ACs—even among batches of a product—play a fundamental role in process variabilities and OMP removals. Hence, ACs are not constantly homogeneous treatment substances, and thus, their characteristics have to be controlled.

Adsorption capacity of ACs is strongly linked to a well-developed pore network and hence internal surface area, originating from AC production processes (carbonization,

activation) at up to 1000 °C (Hernández-Montoya et al. 2012). Carbonaceous raw materials able to withstand such temperatures while developing porosity result in isotropic (not oriented) and non-crystalline structures (Inagaki and Kang 2016). High C content combined with low H or high O contents yields non-graphitizing carbons (no crystalline graphite formed). Many organic raw materials (fossil/regenerative) fulfill these requirements as AC precursors (Mészáros et al. 2007; Menéndez-Diaz and Martin-Gullón 2006). As a result, the raw materials (e.g., coal, plants, crops, sewage sludge) used in thermal or chemical production procedures have become increasingly diverse, with a variety of process parameters (Viegas et al. 2020; Joseph et al. 2020; Danish et al. 2018; Albroomi et al. 2017; Peláez-Cid and Teutli-León 2012; Suhas et al. 2007).

Due to these variations, typical characterizations of ACs solely according to a few selected physical properties (e.g., internal surface area or porosity) fall short of the mark, since the chemical properties of ACs also contribute to adsorption (Piai et al. 2019; Nielsen et al. 2014; Moreno-Castilla 2004; Pendleton et al. 2002). Despite valuable characterizations of individual ACs employing various sophisticated analytical methods (Inagaki and Kang 2016; Durán-Valle 2012; Daud and Houshamnd 2010; Pereira et al. 2003; Rivin 1971), plant operators lack an applicable integration of such analytical information. We therefore suggest thermogravimetric analysis (TGA) as a comparably inexpensive, quick, and robust method. It provides a couple of parameters simultaneously and can be deployed on site for AC quality control and to quantify powdered AC (PAC) in suspension or sludge (Dittmann et al. 2018). TGA is already being applied at mining sites to characterize seam and coal quality as so-called proximate analysis (Speight 2015). The proximate parameters moisture, volatile matter, fixed carbon and ash may imply different and more specific characteristics for ACs.

This paper focuses attention on the surface chemistry of ACs and especially their oxygen-containing functional groups (surface oxygen groups, SOGs), which affect the adsorption of organic molecules in water (Radovic et al. 1997; Franz et al. 2000). Electrostatic attraction or repulsion of a certain ionic or ionizable substance, e.g., by carboxylic acid groups of the AC, depends on the pK_a value(s) of the substance as well as the pH value of the solution and dissolved ions (e.g., Ca^{2+}) (Kah et al. 2017). Hydrogen bonding occurs between all kind of SOGs and respective functional groups of the adsorbate molecule (Tagliavini et al. 2020). Electron donor–acceptor mechanisms can be established by carbonyl groups, but in light of the aromatic carbon structure of AC, this may not be a key mechanism for aromatic moieties of the adsorbate (Franz et al. 2000). However, SOGs also influence dispersive interaction by altering the electron density in graphene π-electron orbitals (Moreno-Castilla 2004), e.g., carboxylic acids decrease the electron density by a negative inductive effect, while phenol and lactone groups increase the electron density by positive mesomeric effects. It has been reported that, for example, phenol groups of AC can chemically react with amide moieties of OMP molecules (Nielsen et al. 2014) and that carbonyl groups influence the adsorption of estradiol (Tagliavini et al. 2020). However, the quantification of SOGs as a relevant material property is rarely applied to commercially available ACs. To fill this gap, we adapted the temperature-programmed decomposition (TPD) methodology (Figueiredo et al. 1999) using TGA coupled to Fourier-transform infrared spectroscopy (TGA-FTIR) (Saal and Dittmann 2021). Not only can the thermal decomposition of a sample provide bulk information as proximate analysis, but in the case of activated carbon TGA-FTIR can also be used to draw conclusions about the surface chemistry.

This study therefore used TGA and TGA-FTIR to examine and compare 25 different AC products along with X-ray fluorescence spectroscopy (XRF) to characterize their inorganic elemental composition. A subset of eight PACs produced from different raw materials and production procedures was selected to broaden the perspective and test for correlations with four commonly used methods of analysis—N_2 adsorption/desorption, CHNS analysis, point of zero charge (PZC) analysis, and X-ray photoelectron spectroscopy (XPS). Furthermore, less commonly utilized methods of analysis, such as particle-size determination and X-ray diffraction spectroscopy (XRD), were conducted, and OMP removals in treated wastewater were determined.

The aims of this study are to: (i) reveal the range of physical and chemical material properties representing characteristics for AC products; (ii) assess TGA mass losses for their surrogate potentials relevant for practitioners; and (iii) quantify and systematize SOGs on ACs depending on their raw materials using TGA-FTIR. Finally, this work is intended to fill in one piece of the puzzle of OMP removal using AC according to appropriate and comprehensive material characterization.

Materials and methods

Figure 1 provides an overview on the study approach with all conducted analyses and methods, which are described below. Additional information on specific handling of the samples can be found in Supplementary Information (SI) A, including particle-size determination, X-ray diffraction spectroscopy (XRD) and discussions on the applicability of certain parameters.
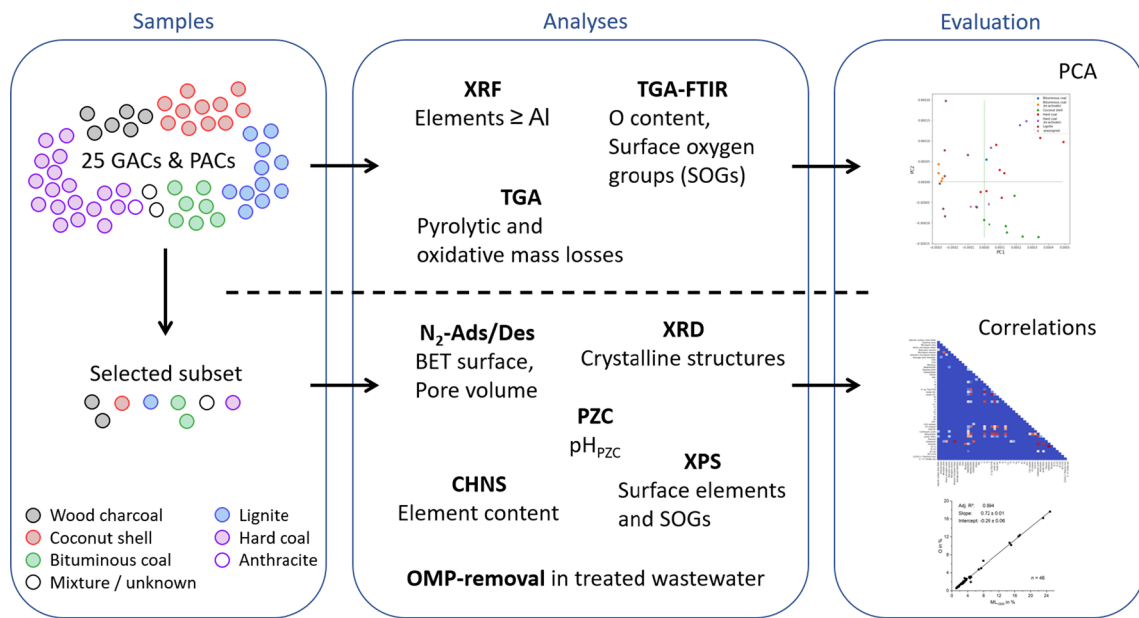
Fig. 1 Scheme of the study approach with activated carbon sample collection, analyses and parameters, and evaluation techniques

Activated carbons

Table 1 lists the eight PACs that underwent all analytical methods conducted. A list of all 25 AC products with batch numbers and milled specimen analyzed using XRF and TGA-FTIR is provided in Table A1 (SI).

Surface area and porosity analyses

N_2 gas adsorption and desorption at 77 K were carried out with an Autosorb-1-MP (Quantachrome Instruments, USA) in duplicate using sample weights of 20–50 mg. Fifty acquisition points in a relative pressure range of 0.010–0.995 were recorded. The software Autosorb for Windows 1.25 and AS1Win 2.11 was used to analyze the isotherm data and to extract information about porosity, surface area, and area of micropore surface and external surface. Detailed information is provided in SI (A).

Carbon, hydrogen, nitrogen, and sulfur (CHNS) analyses

CHNS analysis was conducted using a Thermo FlashEA 1112 Organic Elemental Analyzer with data evaluated using Eager 300 software (Thermo Scientific, USA). We placed defined amounts of 1 mg PAC into a silver capsule that was automatically deployed in a combustion chamber (990 °C) under an excess oxygen atmosphere, with subsequent catalysis of the evolved gases by tungsten trioxide, and nitrous oxide reduction using copper granules. This resulted in the final analyte gases of CO_2, H_2O, N_2, SO_2, detected by zone chromatography with a heat conductivity detector, and a built-in flame photometric detector for SO_2.

It is possible to estimate the oxygen mass content (w_O) of a sample by the difference-to-100% method calculating the difference of the sum of the mass contents of C, H, N, and S, and the ash content on the one hand and the total mass on the other ($w_O = 100\% - w_{CHNS} - w_{Ash}$).

Table 1 Powdered activated carbons that were extensively investigated and the abbreviations used in the following text and figures. 5000 P-f was not analyzed using XPS and XRD due to the limited sample mass

Name	Manufacturer	Raw material	Activation	Abbreviation
HK 950	Carbon Service & Consulting	Wood charcoal	Phosphoric acid	Wood1
HKP 1050	Carbon Service & Consulting	Wood charcoal	Phosphoric acid	Wood2
CCP 90D	Donau Carbon	Coconut shell	Steam	Coco1
SAE Super	Cabot (Norit)	Mixture, Lot 3868836	Unknown	Mix1
5000 P-f	Jacobi Carbons	Lignite	Unknown	Lig1
AZ 1050	Carbon Service & Consulting	Bituminous coal	Unknown	Bitu1
PS-WP 235	Chemviron	Bituminous coal	Unknown	Bitu2
CC 401	Chemviron	Hard coal (reactivate)	Unknown	Hard1

pH at the point of zero charge (PZC)

The PZC was determined using a pH drift method (Müller et al. 1985), in line with recent literature (Rivera-Utrilla et al. 2001; Dittmar et al. 2018). In short, 50 mg of each PAC was placed in flasks containing 150 mL of a 0.01 M NaCl solution, with pH adjusted prior to use (3, 4,…, 11). After 23-h equilibrium time, the resulting pH values were measured and plotted against the initial pH values. The PZC was determined by linearly interpolating between the two adjacent data points whose linear connection intersected with the bisector. Extrapolation was used for Mix1 whose PZC exceeded 11, since pH = 11 was the highest initial pH applied.

X-ray photoelectron spectroscopy (XPS)

X-ray photoelectron spectroscopy (XPS) was performed using a SAGE 100 device (Specs, Germany). Aluminum $K\alpha$ radiation (1486.6 eV) was used to excite the photoelectrons at 20 mA and 10 kV under an ultra-high vacuum ($< 3 \cdot 10^{-7}$ mbar). At least two replicates were measured before calculating mean values for the element contents. The spectra were analyzed using SpecsLab and fitted using CasaXPS. The C–C bond was used for standardization with a binding energy of 285 eV. Peak fitting was performed for C=O, C=O, O–C=O and carbonate in accordance with Desimoni et al. (1990) and Durán-Valle (2012). Additional information can be found in SI (A).

X-ray fluorescence spectroscopy (XRF)

Energy-dispersive X-ray fluorescence spectroscopy (XRF) was performed on a Spectro XEPOS III using X-LabPro 5.1/TurboQuant software (Spectro Analytical Instruments, Germany) on sample masses of at least 1 g. The TurboQuant method applies the fundamental parameters method for the semi-quantitative analysis of elements ranging from aluminum to uranium. Additional details about the method are provided in SI (A).

Thermogravimetric analysis (TGA)

For temperature-controlled decomposition of the samples, a thermobalance TGA/DSC 3+ from Mettler Toledo (USA) with a purge gas flow of 50 mL min^{-1} was used (see SI (A) for details). The continuous TGA data obtained as mass loss or TG curve were further differentiated according to measurement time, which yielded mass loss rates or a DTG curve. Specific mass losses were normalized to dry sample mass (145 °C) and consist of pyrolytic mass loss up to 600 °C (ML_{600}) and up to 1000 °C (ML_{1000}) in a nitrogen atmosphere and of oxidative mass loss ($ML_{ox.}$) in synthetic air. The latter is calculated by subtracting the mass residue after oxidation (ash) at 900 °C and ML_{1000} of 100%.

Thermogravimetry coupled to Fourier-transform infrared spectroscopy (TGA-FTIR)

To determine the so-called surface oxygen groups (SOGs) and the oxygen content of the samples, we coupled the TGA to a Fourier-transform infrared spectrometer to conduct continuous evolved gas analysis. A Nicolet iS50 was used with a DTGS detector as well as a TG-IR module consisting of a heated transfer line (250 °C) and IR cell (260 °C) from Thermo Fisher Scientific (USA). TGA-FTIR measurements were taken in triplicate in a nitrogen atmosphere up to 1000 °C. FTIR spectra were analyzed for H_2O, CO_2, CO, and CH_4 to derive gas-specific release rates (OMNIC 9.7.39 software). H_2O, CO_2, and CO were quantified using previous calibration with calcium oxalate monohydrate (purity 99.9985%, Alfa Aesar, USA) that allows to determine the oxygen content and the SOG quantities.

According to temperature-programmed decomposition (TPD) methodology, individual SOGs in carbon materials decompose to H_2O, CO_2, or CO in certain temperature ranges (Figueiredo et al. 1999). These ranges overlap, but can be distinguished by deconvolution by fitting Gaussian curves. After reviewing the literature and analyzing the ACs, we adapted a TPD method for the TGA-FTIR setup (Table 2). A Python package for the quantification of SOGs by TGA-FTIR has been developed that includes a robustness test of the fitting (Saal and Dittmann 2021). Variation of the initial parameters to certain extents provides mean values

Table 2 Assignment of CO_2, CO, and H_2O to surface oxygen groups released at certain temperatures (in °C)

	CO_2	CO	H_2O
Adsorbed	95	–	90
Unassigned 1	–	–	210[a]
Unassigned 2	–	–	255[a]
Carboxylic acids 1	245	255	–
Carboxylic acids 2	380	410	–
Anhydrides	500*	530*	–
Unassigned CO_2	625[b]	–	–
Lactones 1	635	–	–
Lactones 2	785	–	–
Phenols	–	670	–
Carbonyls 1	–	790	–
Carbonyls 2	–	870	–
Pyrones	–	960	–

[a]unassigned H_2O releases found from Wood1 and Wood2; [b]unassigned CO_2 release found from Hard1; *CO release predefined by quantity of the respective CO_2 release (by width and height of fitted Gauss curves)

with standard deviations as uncertainty. See SI (A) for more comprehensive details also on method development.

Adsorption experiments

Wastewater treatment plant effluent (conventional mechanic-biological treatment with biological P elimination, dry weather capacity ca. 105,000 m^3 day^{-1}, DOC = 10.3 mg L^{-1}) was used to examine OMP adsorption onto eight selected PACs (Table 1). Fifteen OMPs were additionally spiked to increase their concentration approx. fivefold. This facilitates analyses using HPLC-MS/MS and determination of relative removals, but does not influence competition conditions significantly (Zietzschmann et al. 2016a, b). PAC doses of 10 and 20 mg L^{-1} were applied in batch experiments of 100 mL volume. 48 h contact time on a horizontal shaker ensures obtaining the adsorption equilibrium prior to filtration. Uncertainty of the results is given as standard deviation of ten reference samples treated as described above but without any PAC dosage. Further details are provided in SI (A).

Principal component analysis

Principal component analysis (PCA) reduces the number of dimensions (or elements in the case of XRF) by aggregating them into principal components (PCs) according to their largest variances, thus emphasizing differences in the compositions. PCA was applied to the XRF and TGA-FTIR (SOGs) results, using a Python script with the PCA class and normalize function from the scikit-learn package (v. 0.23.2) (Pedregosa et al. 2011).

Results and discussion

Physical (surface) morphology

The internal morphology of AC adsorbents is usually determined by pore volume, BET surface (specific surface area, SSA), and pore size distribution (PSD). These parameters are derived from gas adsorption/desorption isotherms typically determined using N_2 at the boiling point. However, since the informational value of this basic data may be overlooked, shapes and details on the isotherms with IUPAC classification (Thommes et al. 2015) are provided in the SI (Table B1 and Figs. B1–B3).

The PACs under examination are mesoporous carbons with several pore sizes and with a remarkable share of micropores, except for Coco1, which is a microporous carbon with narrow mesopores. Quantitative values for total pore volume and SSA with respective shares of micropores, mesopores, and macropores for the eight PACs are shown in Fig. 2. The specific micropore surface area does
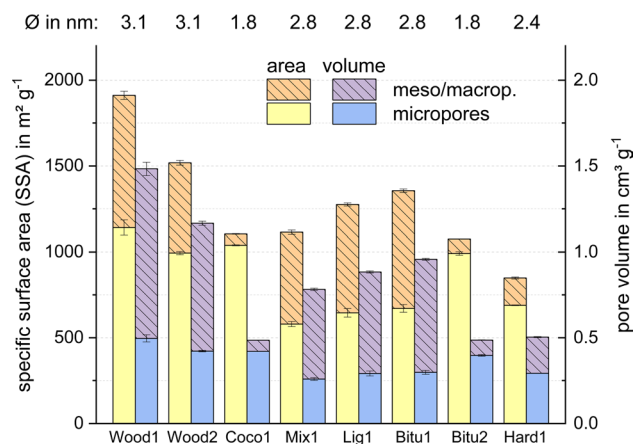
Fig. 2 Specific surface area (SSA) and total pore volume of the eight PACs with respective shares of mesopores, macropores, and micropores, with average pore diameters (4 V/A) on top

not correlate with the overall SSA (cf. Wood2 and Coco1), and the variations in SSA and total pore volume are less pronounced with respect to micropores. In accordance with the N_2 adsorption/desorption isotherms (Fig. B1), more differences can be seen in the proportions of the mesopores. These absolute distinctions are not reflected in the average pore diameter (Fig. 2, top), because this is calculated by the ratio of total pore volume to SSA and multiplying by a factor of 4. The parameter called "hydraulic" or "4 V/A" average pore diameter therefore assumes a cylindrical pore geometry and does not represent a feature of the PSD, but rather is related to the share of micropores. Since the pore network of an AC is more complex, this parameter should be used carefully. A comment on ACs and PSDs based on density function theories is given in SI (Figs. B4–B5).

In conclusion, N_2 adsorption/desorption isotherms are well suited for the qualitative comparison of AC products regarding their (meso-)pore network, which is crucial with respect to the adsorption of large molecules from dissolved organic matter and to adsorption kinetics. SSA and total pore volume with respective micropore and mesopore proportions provide valuable quantitative information on an AC product's porosity and its potential adsorption capacity for adsorbate molecules. However, these physical morphology characteristics are not sufficient for estimating the adsorption of specific molecules, apart from their steric access to the pores (Piai et al. 2019; Nielsen et al. 2014; Moreno-Castilla 2004); nor for obtaining information about the raw material of the AC product at hand. The chemical composition may reveal more insights, such as carbon content for dispersive interaction, oxygen content for hydrogen bonding, or even inorganic elements for ion binding.

Chemical composition

Common tools for the quantification of elements that comprise the carbon structure include CHNS analysis by thermal oxidation of the sample, as well as XPS or additional ash content determination to estimate the oxygen content. The mass content of carbon in the eight PACs ranges between 75% and 92%, as listed in Table 3. The hydrogen contents of approx. 2% in the chemically activated PACs (Wood1 and Wood2) is a magnitude above that of the others. Nitrogen and sulfur, with a maximum content of 0.22% and 0.35% (Hard1), respectively, were not detected in all samples.

The oxygen content considerably differs when calculated using the difference-to-100% method or X-ray photoelectron spectroscopy (XPS), as the oxygen content is not covered by the CHNS analysis (Table 3). Furthermore, XPS has frequently been used to determine surface oxygen groups (SOGs), since it can distinguish C–O, C=O, and O–C=O bonds. With regard to the high surface sensitivity of XPS (outer particle surface) and the enhanced oxidation found, XPS results are probably not representative of the total SOGs (see SI (B, Sect. 1.4.3) for details).

The point of zero charge (PZC) is an important parameter for the adsorption of ionic or ionizable molecules (Kah et al. 2017). Table 3 shows that it ranges from a very low pH 2.8 for the chemically activated PACs to neutral and alkaline pH values. Delocalized π-electrons of basal planes of the ACs' carbon structures accept H^+ somewhat and therefore provide large non-heteroatomic Lewis base sites (Bandosz and Ania 2006). As the oxygen content increases (or SOGs), the PZC decreases due to acidic functional groups as well as due to inductive and mesomeric effects that reduce the π-electron density (Deng et al. 2014). However, the pure oxygen content obtained in this study did not correlate with the PZC, which could be due to different relative SOG compositions, also regarding the connection of SOGs to other elements (e.g., S or P).

The inorganic elemental composition is primarily composed of Al, Si, P, S, K, Ca, and Fe. Sodium and magnesium cannot be detected by X-ray fluorescence spectroscopy

(XRF). The ash content is not related to the elemental composition (Fig. B8, SI), but probably determined by burn-off mass losses during production and, to a lesser extent, by the ash content of the raw material. Find structural analyses by X-ray diffraction (XRD) and transmission electron microscopy (TEM) in SI (B), since adsorption mechanisms are probably not significantly influenced by crystalline phases.

However, principal component analysis (PCA) reveals similarities and differences in the inorganic elemental composition (which had been determined using XRF) of 35 samples, as shown in Fig. 3. The results clearly indicate several clusters of similar inorganic elemental compositions. The two clusters on the left-hand side mainly include ACs
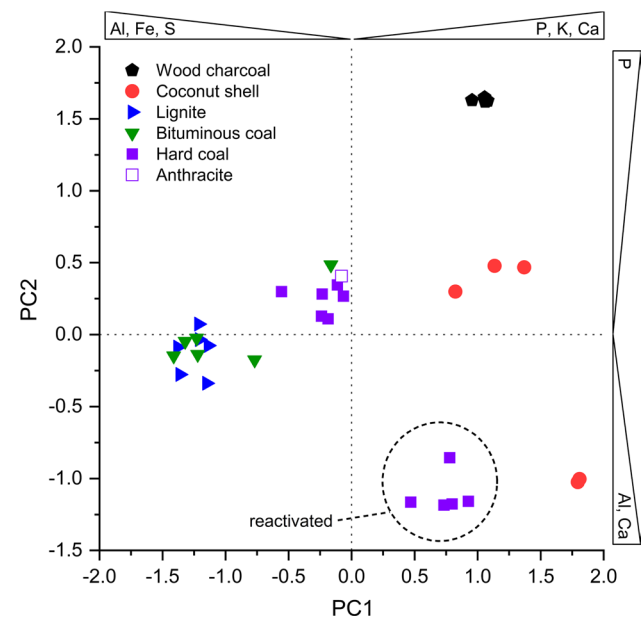
Fig. 3 Score plot of the principal component analysis (PCA) with points representing 34 ACs (GACs and PACs) and anthracite, analyzed by X-ray fluorescence spectroscopy (XRF). Elements contributing the most to principal components (PC) 1 and 2 are indicated at the top and on the right-hand side, specific contributions (loadings) are provided in SI (Fig. B20)

Table 3 Elemental composition of carbon, hydrogen, nitrogen, sulfur, and oxygen and the point of zero charge (PZC) for the eight PACs

	Analysis	Unit	Wood1	Wood2	Coco1	Mix1	Lig1	Bitu1	Bitu2	Hard1
C	CHNS	wt%	80.5 ± 0.8	75.0 ± 0.0	90.3 ± 2.4	79.0 ± 0.6	79.5 ± 1.3	84.7 ± 0.8	92.2 ± 1.2	83.4 ± 1.9
C	XPS	wt%	81.4	73.5	76.3	72.7	n.d.	78.5	89.1	89.0
H	CHNS	wt%	2.16 ± 0.20	2.06 ± 0.30	0.28 ± 0.15	0.14 ± 0.09	0.17 ± 0.10	0.35 ± 0.29	0.45 ± 0.07	0.21 ± 0.11
N	CHNS	wt%	0.08 ± 0.01	0.22 ± 0.01	–	–	0.04 ± 0.01	0.04 ± 0.01	0.10 ± 0.02	0.22 ± 0.02
S	CHNS	wt%	–	–	–	0.16 ± 0.06	–	0.11 ± 0.03	–	0.35 ± 0.04
O	$100\% - w_{CHNS} - w_{Ash}$	wt%	13.6	16.1	5.3	4.6	7.4	6.7	3.7	3.0
O	XPS	wt%	14.2	19.3	11.3	12.7	n.d.	9.7	10.9	11.0
PZC	pH drift	pH	3.3	2.8	9.1	11.4	7.3	8.4	9.5	9.7

made of hard coal, lignite, or bituminous coal. These clusters separate due to the large aluminum content in the lignite samples (cf. SI, Fig. B8). AC products made of bituminous coal are found in both clusters, probably due to different qualities. Sub-bituminous coal has lignite characteristics, and bituminous coal is comparable to hard coal. ACs at the bottom of the score plot, e.g., reactivated GACs from hard coal, revealed an increased relative calcium content. Chemically activated AC products made of wood charcoal cluster at the top due to their high phosphorous mass shares. The ACs made of coconut shell exhibited a separate cluster due to their potassium content. However, some of these samples also had a high calcium contents, which is why they were also separated from the primary coconut shell cluster.

In conclusion, the relative elemental composition of inorganic elements clearly represents the AC products' raw materials and activation procedures. These findings may help to classify unknown AC products. The PCA is published along with the experimental raw data (Dittmann et al. 2022) and can be expanded to include additional samples. Furthermore, the crucial oxygen content does not appear to be conclusively determined by the difference-to-100% method or by XPS, nor do the SOGs appear to be conclusive. It therefore made more sense to use the alternative methods of TGA and TGA-FTIR to characterize the bulk AC particles.

Oxygen and carbon content

AC samples primarily release CO_2, CO, and, if present, H_2O during pyrolysis. This is due to the decomposition of SOGs and is accompanied with the pyrolytic mass loss during TGA up to 1000 °C (ML_{1000}). The oxygen mass content determined by TGA-FTIR is therefore found to correlate very well ($R^2 = 0.994$) with ML_{1000} (Fig. 4).

This means that ML_{1000} is a good surrogate parameter for the oxygen content of ACs using the factor 0.72 (slope). It should be noted that the six chemically activated ACs made of wood charcoal obtained the highest values by far for ML_{1000} (and ML_{600}) or oxygen, respectively. In contrast, the majority of samples had an oxygen mass content below 3% (Fig. 4). However, the correlation and slope also apply to the samples with low oxygen content. The effect that grinding GAC has on oxygen content is provided and discussed in SI (B, Sect. 1.3.2).

Additional correlations can be drawn with the properties determined for the eight PACs (Fig. 5). Mass loss during oxidation ($ML_{ox.}$) was correlated to the carbon content by $R^2 = 0.952$ (Fig. 5a). It is important to note that $ML_{ox.}$ is caused by the elements carbon and hydrogen and that carbon is also a part of the strictly pyrolytic mass loss ML_{1000} (no oxygen, thus no oxidation) released as CO_2 and CO. Proximate analysis therefore applies the term "fixed carbon"
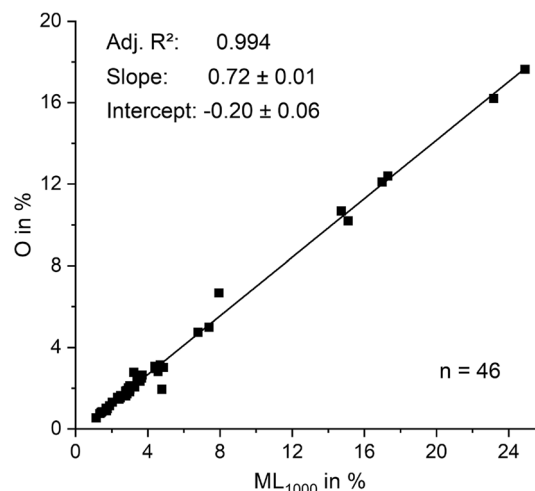
Fig. 4 Linear correlation of the pyrolytic mass loss up to 1000 °C (ML_{1000}) and the oxygen mass content determined by TGA-FTIR

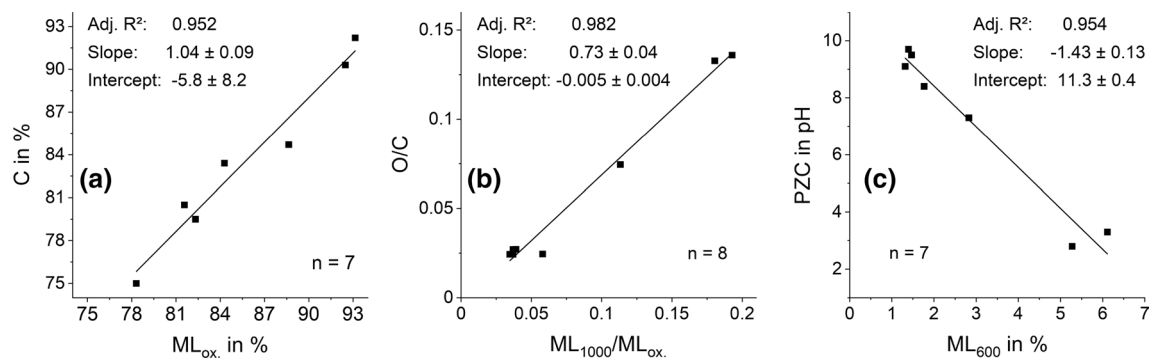for the oxidative mass loss after pyrolysis (Speight 2015). The ratio of ML_{1000} to $ML_{ox.}$ can function as a surrogate for the O/C ratio, which indicates the hydrophilic character of an AC, due again to a very close correlation ($R^2 = 0.982$, Fig. 5b). Acidic functional groups (carboxylic acid, anhydride, and lactone groups) of the SOGs decompose into CO and CO_2 at lower temperatures (cf. Table 2). The pyrolytic mass loss up to 600 °C (ML_{600}) was therefore found to correlate with the point of zero charge (PZC) by $R^2 = 0.954$ (Fig. 5c).

The PAC Mix1 was omitted from correlations with C and PZC because its high calcite content would otherwise distort the results. This limitation can be ascertained by evaluation of the mass loss rates, since DTG curves indicate the decomposition of carbonates between 600 and 700 °C as a distinctive peak (Fig. 6, Bitu2). For example, for Mix1, this peak represents a mass loss of 4.9% (Fig. B23, SI); if this is attributed to the release of CO_2 from the decomposition of calcite ($CaCO_3$) into calcium oxide (CaO), the calculated result should be 11.2% calcite (4.5% calcium) in the sample and 6.3% CaO in the ash. Furthermore, these values can be used to clarify the carbon and oxygen content as well as the PZC in advance, such as via Mix1.

In conclusion, standalone TGA analyses are adequate for representing AC properties and for providing mass loss profiles (DTG curves) of pyrolysis. The latter not only indicates calcite or carbonate impurities, but also depicts the product-specific chemistry via the decomposition of SOGs released as CO_2 and CO.

Oxygen-containing functional groups

We used TGA-FTIR to determine the CO_2 and CO release rates, which in turn allowed us to determine specific SOGs

Fig. 5 Linear correlations of **a**: the oxidative mass loss and the carbon mass content determined by CHNS analysis, **b**: the O/C ratio and the respective ratio of the surrogates, and **c**: the pyrolytic mass loss up to 600 °C (ML_{600}) and the point of zero charge (PZC)

Fig. 6 Mass loss profiles (DTG curves) of Coco1, Bitu1, Bitu2, and Hard1 in multiple determinations. DTG curves for Wood1, Wood2, Mix1, and Lig1 are provided in SI (Fig. B23)
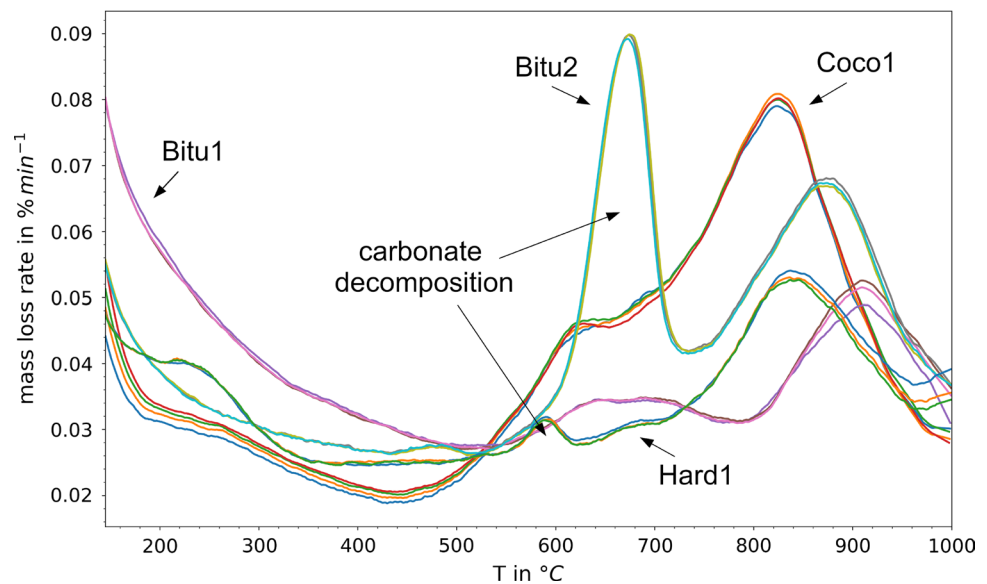
by deconvolution. Of the 48 samples analyzed, only two could not be properly fitted (including Mix1; relative squared error of the fit > 0.4%). This might be related to high ash and calcium content affecting the thermal decomposition at lower temperatures (Várhegyi et al. 1997). Fig. 7 shows examples of deconvolutions of the release rates of Hard1. Carboxylic acids and carboxylic anhydrides decompose below 600 °C. Both groups are acidic and of special interest with regard to the adsorption of polar or charged substances (cf. ML_{600} in previous Section). The example includes a sharp CO_2 peak at about 600 °C, which can be attributed to the decomposition of carbonates (cf. Fig. 6). This peak was fitted by an additional "unassigned-CO2" peak and is therefore not attributed to SOG. However, if there is more CO_2 that has evolved from carbonates, this may not be intercepted by a Gaussian-shaped "unassigned-CO2" peak. In such cases, the deconvolution was only evaluated up to 600 °C.

Furthermore, the evaluation must be limited to 600 °C if methane evolves above this temperature. Methane evolution indicates carbonization reactions, and the CO_2 and CO released cannot be fully assigned to SOGs. All chemically activated ACs released methane, probably due to the comparably low activation temperature that restricts carbonization reactions during production.

In summary, six SOGs were obtained for 34 samples, two SOGs (carboxylic acids and anhydrides) were determined for 12 samples, and two samples had to be excluded. Furthermore, the evolution of CO at very high temperatures was disturbed by inevitable oxidation reactions (for details, see Sect. 1.7.3 in the SI (A)). The quantity of pyrone groups is therefore overestimated, but their fit was reproducible, nevertheless. TGA-FTIR results with evolved gas profiles and deconvolution figures of all samples are provided with the experimental raw data (Dittmann et al. 2022).

The raw material is expected to affect the nature of the chemistry, in terms of the absolute SOG composition as

Fig. 7 Deconvolution of CO_2 (top) and CO (below) release rates of Hard1 with deviations (errors) between recorded data and resulting fit from the deconvolution with Gaussian peaks
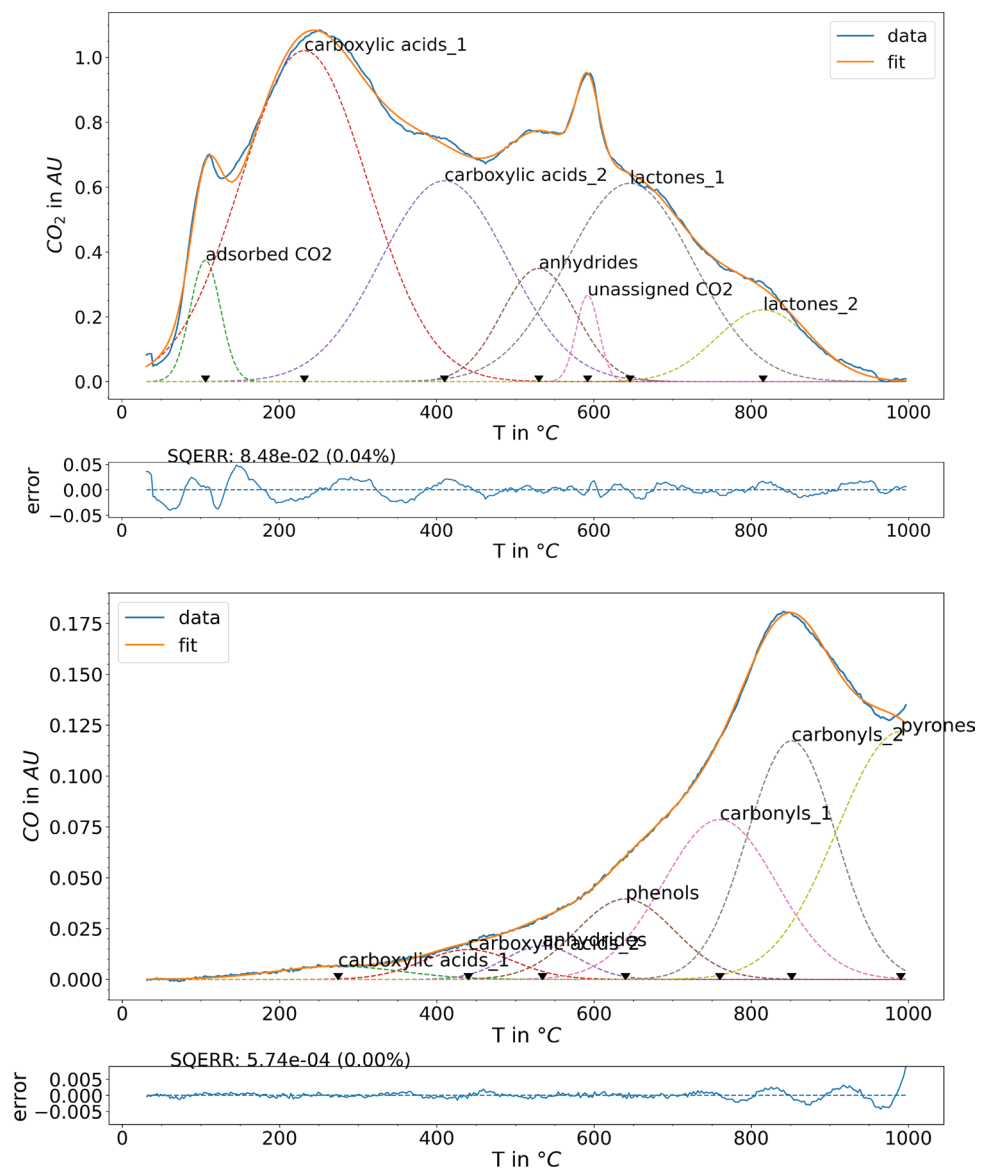

well as the relative SOG composition in a sample. The SOG quantities of the ACs presented as box plots in Fig. 8 are therefore grouped according to the respective raw materials. High levels of a wide range of carboxylic acids were found for AC products made of wood charcoal. It is likely that their chemical activation with phosphoric acid leads to the high content of acidic SOGs. Furthermore, high quantities of carbonyl groups were found, while a low content of anhydrides and lactone groups was determined. ACs made from coconut shell show a comparably high content of carboxylic acid groups compared to AC products from fossil precursors. ACs made from hard coal and their reactivates exhibit higher amounts of carbonyl and pyrone groups. ACs from lignite and bituminous coal and their reactivates contain fewer carbonyl groups and more pyrone groups than carbonyl groups. For hard coal and coconut shell, it is the other way around.

These findings are also supported by two PCAs provided in SI (Figs. B33–B36).

Finally, let us return to the eight PACs we selected for comprehensive characterization. The determination of the specific SOGs can explain the low PZC of the wood charcoal products Wood1 and Wood2. Also, the inconsistencies in the correlation between PZC and oxygen content can be attributed to the different relative SOG composition of the PACs (cf. SI, Figs. B25 and B26).

In conclusion, the chemistry of AC products depends to some extent on the raw material and can be quantified using a TGA-FTIR setup. Different SOGs very likely influence the adsorption of specific target compounds and therefore offer the opportunity to select AC products based on their surface chemistry. However, the impact of
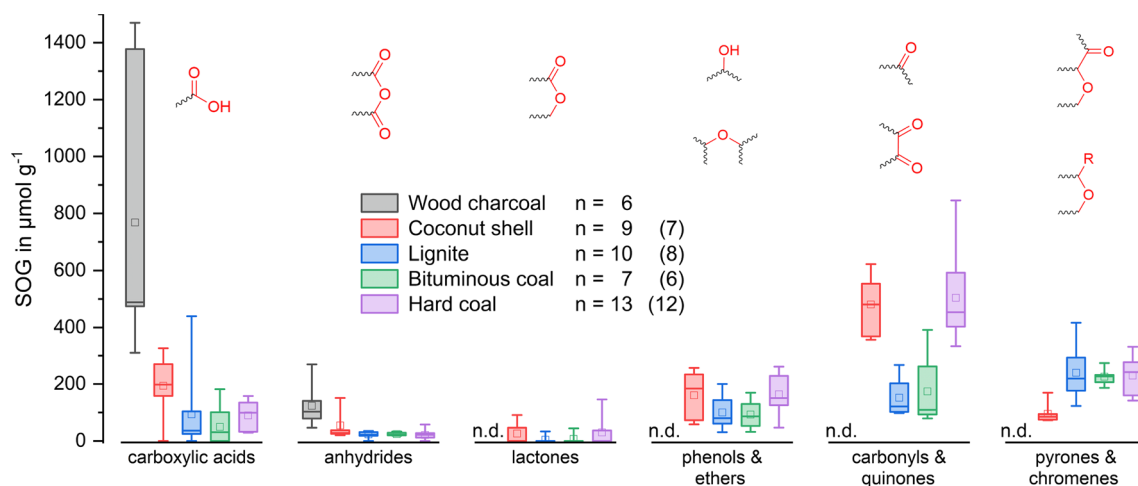
Fig. 8 Box plots grouped by SOGs and subgrouped by the raw material of ACs with whiskers representing the span; boxes include 50% of the results; means are given as squares and medians as horizontal bars. The number of measurements (*n*) is given for carboxylic acids and anhydrides in each subgroup; the number in parentheses refers to the remaining SOGs

the SOG contents on OMP elimination in real water still requires clarification.

Adsorption mechanisms in real water

Figure 9 shows removals for carbamazepine, diclofenac, and benzotriazole from treated wastewater (high DOC can result in strong adsorption competition) for the eight PACs, obtained in batch experiments.

Carbamazepine is removed by all types of PACs above 80% already at the lower PAC dose of 10 mg L^{-1}. The detailed composition of SOGs is of minor importance. This confirms carbamazepine as strong adsorbate even in competitive conditions. Furthermore, the eight PAC products provide adsorption sites with high affinity to this kind of molecule. It is therefore most likely that the dominant adsorption interactions are dispersive forces. They occur between the aromatic carbon structures (graphite, graphene) present in high content in all PACs and the dibenzazepine moiety of the adsorbate molecule with a flat structure (Dittmann et al. 2020).

Diclofenac is removed to different extents. The removal of the anionic diclofenac suffers from DOC competition on Coco1, Bitu2, and Hard1 at low PAC dose. Doubling the PAC dose increases the removal of diclofenac to above 80%. Coco1, Bitu2, and Hard1 have the lowest volume of mesopores and macropores. They also own the highest relative content of ketones and carbonyls. The three-dimensional structures of these SOGs indicate a derivation of the stacked layer structure of graphite, in contrast to the carboxylic acids, anhydrides, lactones, ethers, and chromenes, which can be integrated in the stacked layer structure of graphite. Diclofenac has a three-dimensional structure, while carbamazepine is a flat molecule. High volumes of meso- and macropores support the adsorption process, and adsorption sides provide space for three-dimensional structures. It is noteworthy that the acidic character of diclofenac (and thus a possible ionic interaction) does not seem to be relevant to the overall adsorption process in real water.

Benzotriazole is also removed to different extents. Benzotriazole is removed the best by Coco1, Bitu2, and Hard1, and the PACs Wood1 and Wood2 do not achieve 60% removal even with the higher dose of 20 mg L^{-1}. Compared to carbamazepine and diclofenac, benzotriazole is a relatively small molecule with a flat structure. Therefore, the dominant aromatic structures of the ACs are expected to dominate the adsorption process (like for carbamazepine), and the missing of large pore volume and non-plane artefacts in graphite will not reduce the removal rate (like for diclofenac). However, sorption behavior of benzotriazole does not fit to this prediction. We conclude that in this case the amphoteric character of the triazole ring suppresses the sorption and the aromatic interaction of only one ring is not sufficient for a meaningful π-π interaction.

In conclusion, mechanisms in play are dependent on an OMP specific *combination* of the AC material properties and the composition of the water matrix. SOGs can be involved via several adsorption mechanisms. The present study offers new possibilities by TGA and TGA-FTIR to examine more detailed chemical properties and may therefore facilitate mechanistic investigations and model development.
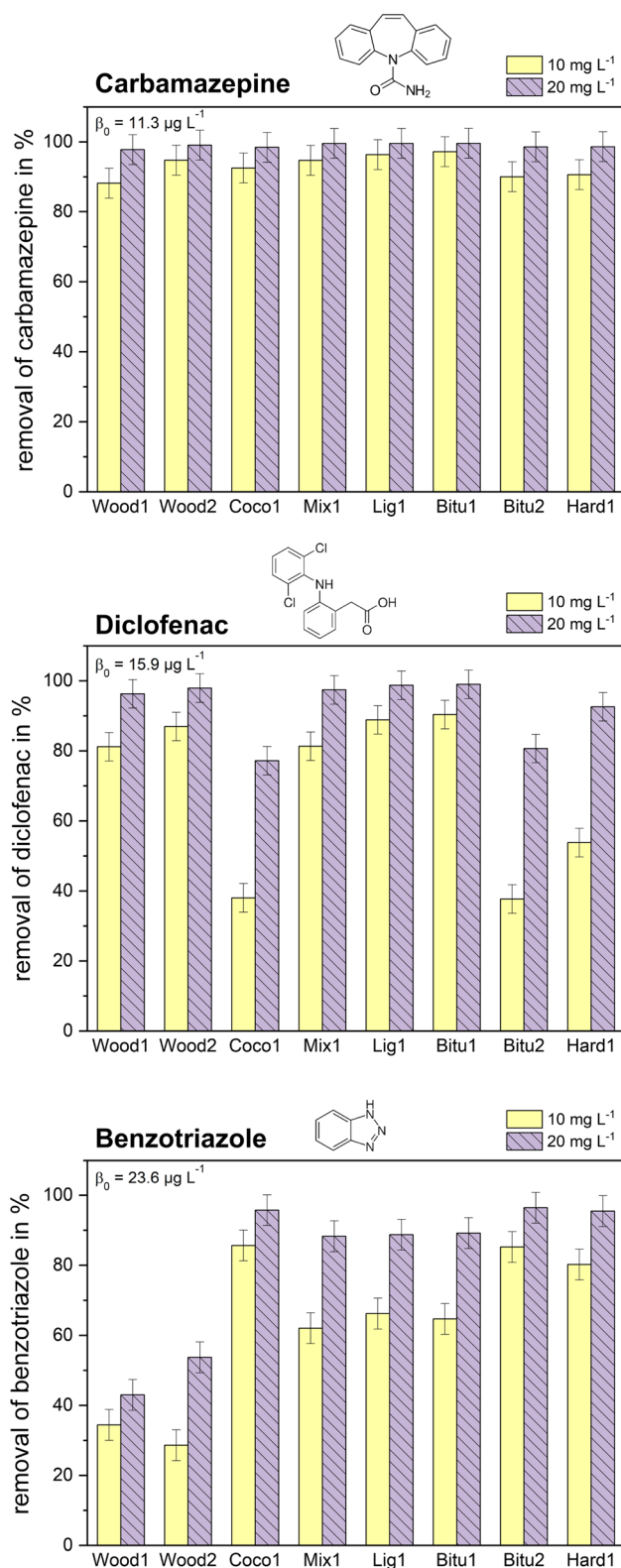
Fig. 9 Selected removals of carbamazepine, diclofenac and benzotriazole in treated wastewater for the eight PACs, each dosed as 10 mg L^{-1} and 20 mg L^{-1}

Conclusion

ACs showed large variations in their physical and chemical properties, probably due to different raw materials and activation procedures, both of which affect porosity development, elemental composition, and the surface chemistry of the product.

The elemental composition of inorganic impurities was shown to be closely related to the raw material and the activation process of the AC, thus allowing for classification of unknown samples.

Thermogravimetric analysis (TGA) provides surrogate information on the point of zero charge (ML_{600}), the oxygen content (ML_{1000}), the carbon content ($ML_{ox.}$), and the derived O/C ratio. Derivative thermogravimetry (DTG) curves provide a chemical fingerprint of an AC. The oxygen content of an AC sample is more conclusively represented by its pyrolytic mass loss up to 1000 °C (ML_{1000}) than by estimation from CHNS analysis using ash content or by XPS analysis. Six types of oxygen-containing functional groups (SOGs) occur in different levels and contribute to significant differences among AC products. Chemically activated wood charcoals exhibit great quantities of carboxylic acids, whereas coconut shell and hard coal-based ACs are dominated by carbonyl groups; AC products made from lignite or bituminous coal imply lower SOG levels, mostly represented by carbonyl and pyrone groups.

Generating appropriate material characterizations of ACs using TGA and TGA-FTIR may fill in a missing piece of the puzzle when predicting organic micropollutant removals by AC and will become even more crucial with increasing amounts of renewable products from diverse precursors, such as biochars, waste-derived carbons, and other lignocellulosic or carbonaceous materials. Looking ahead, a comprehensive analysis of individual OMP removals in real water, together with the AC properties studied here, is highly appropriate. This would potentially allow the deduction of key mechanisms of adsorption in complex water matrices.

Availability of data and materials The experimental raw data and processed data on which this article is based are made available in a Zenodo repository (Dittmann et al. 2022).

Code availability The Python package used to evaluate the TGA-FTIR data is available at GitHub (Saal and Dittmann 2021).

Declarations

Conflict of interest The authors have no competing interest to declare that are relevant to the content of this article.

Consent to participate The authors give their consent for participation and publication.

Ethical approval Not applicable

References

Albroomi HI, Elsayed MA, Baraka A et al (2017) Batch and fixed-bed adsorption of tartrazine azo-dye onto activated carbon prepared from apricot stones. Appl Water Sci 7(4):2063–2074. https://doi.org/10.1007/s13201-016-0387-2

Bandosz TJ (ed) (2006) Activated carbon surfaces in environmental remediation, vol 7, 1st edn. Elsevier, New York

Bandosz TJ, Ania CO (2006) Surface chemistry of activated carbons and its characterization. In: Bandosz TJ (ed) Activated carbon surfaces in environmental remediation, vol 7. Elsevier, New York, pp 159–229

Danish M, Ahmad T, Nadhari WNAW et al (2018) Optimization of banana trunk-activated carbon production for methylene blue-contaminated water treatment. Appl Water Sci 8(1):9. https://doi.org/10.1007/s13201-018-0644-7

Daud WMAW, Houshamnd AH (2010) Textural characteristics, surface chemistry and oxidation of activated carbon. J Nat Gas Chem 19(3):267–279. https://doi.org/10.1016/S1003-9953(09)60066-9

Deng JP, Chen WH, Chiu SP et al (2014) Edge-termination and core-modification effects of hexagonal nanosheet graphene. Molecules 19(2):2361–2373. https://doi.org/10.3390/molecules19022361

Desimoni E, Casella GI, Morone A et al (1990) XPS determination of oxygen-containing functional groups on carbon-fibre surfaces and the cleaning of these surfaces. Surf Interface Anal 15(10):627–634. https://doi.org/10.1002/sia.740151011

Dittmann D, Braun U, Jekel M et al (2018) Quantification and characterisation of activated carbon in activated sludge by thermogravimetric and evolved gas analyses. J Environ Chem Eng 6(2):2222–2231. https://doi.org/10.1016/j.jece.2018.03.010

Dittmann D, Eisentraut P, Goedecke C et al (2020) Specific adsorption sites and conditions derived by thermal decomposition of activated carbons and adsorbed carbamazepine. Sci Rep 10(1):6695. https://doi.org/10.1038/s41598-020-63481-y

Dittmann D, Saal L, Zietzschmann F et al (2022). Experimental raw data for Characterization of activated carbons for water treatment using tga-ftir for analysis of oxygen-containing functional groups. https://doi.org/10.5281/zenodo.4923133

Dittmar S, Zietzschmann F, Mai M et al (2018) Simulating effluent organic matter competition in micropollutant adsorption onto activated carbon using a surrogate competitor. Environ Sci Technol 52(14):7859–7866. https://doi.org/10.1021/acs.est.8b01503

Durán-Valle CJ (2012) Techniques employed in the physicochemical characterization of activated carbons. In: Lignocellulosic precursors used in the synthesis of activated carbon - characterization techniques and applications in the wastewater treatment. IntechOpen, pp 37–55

Figueiredo JL, Pereira MFR, Freitas MMA et al (1999) Modification of the surface chemistry of activated carbons. Carbon 37(9):1379–1389. https://doi.org/10.1016/S0008-6223(98)00333-9

Franz M, Arafat HA, Pinto NG (2000) Effect of chemical surface heterogeneity on the adsorption mechanism of dissolved aromatics on activated carbon. Carbon 38(13):1807–1819. https://doi.org/10.1016/S0008-6223(00)00012-9

Golovko O, de Brito Anton L, Cascone C et al (2020) Sorption characteristics and removal efficiency of organic micropollutants in drinking water using granular activated carbon (GAC) in pilot-scale and full-scale tests. Water 12(7):2053. https://doi.org/10.3390/w12072053

Guillossou R, Le Roux J, Mailler R et al (2019) Organic micropollutants in a large wastewater treatment plant: What are the benefits of an advanced treatment by activated carbon adsorption in comparison to conventional treatment? Chemosphere 218:1050–1060. https://doi.org/10.1016/j.chemosphere.2018.11.182

Hernández-Montoya V, García-Servin J, Bueno-López JI (2012) Thermal treatments and activation procedures used in the preparation of activated carbons. In: Lignocellulosic precursors used in the synthesis of activated carbon - characterization techniques and applications in the wastewater treatment

Joseph B, Kaetzl K, Hensgen F et al (2020) Sustainability assessment of activated carbon from residual biomass used for micropollutant removal at a full-scale wastewater treatment plant. Environ Res Lett 15(6):064. https://doi.org/10.1088/1748-9326/ab8330

Kah M, Sigmund G, Xiao F et al (2017) Sorption of ionizable and ionic organic compounds to biochar, activated carbon and other carbonaceous materials. Water Res 124:673–692. https://doi.org/10.1016/j.watres.2017.07.070

Menéndez-Diaz JA, Martin-Gullón I (2006) Types of carbon adsorbents and their production. In: Bandosz TJ (ed) Activated carbon surfaces in environmental remediation, vol 7. Elsevier, New York, pp 1–47

Mészáros E, Jakab E, Várhegyi G et al (2007) Do all carbonized charcoals have the same chemical structure? 1. Implications of thermogravimetry-mass spectrometry measurements. Ind Eng Chem Res 46(18):5943–5953. https://doi.org/10.1021/ie0615842

Michio Inagaki, Feiyu Kang (2016) Materials science and engineering of carbon. Elsevier. https://doi.org/10.1016/C2014-0-03769-0

Moreno-Castilla C (2004) Adsorption of organic molecules from aqueous solutions on carbon materials. Carbon 42(1):83–94. https://doi.org/10.1016/j.carbon.2003.09.022

Müller G, Radke CJ, Prausnitz JM (1985) Adsorption of weak organic electrolytes from dilute aqueous solution onto activated carbon. Part I. Single-solute systems. J Colloid Interface Sci 103(2):466–483. https://doi.org/10.1016/0021-9797(85)90123-7

Nielsen L, Biggs MJ, Skinner W et al (2014) The effects of activated carbon surface features on the reactive adsorption of carbamazepine and sulfamethoxazole. Carbon 80:419–432. https://doi.org/10.1016/j.carbon.2014.08.081

Pedregosa F, Varoquaux G, Gramfort A et al (2011) Scikit-learn: machine learning in python. J Mach Learn Res 12(85):2825–2830

Peláez-Cid AA, Teutli-León MMM (2012) Lignocellulosic precursors used in the elaboration of activated carbon. In: Lignocellulosic precursors used in the synthesis of activated carbon - characterization techniques and applications in the wastewater treatment. https://doi.org/10.5772/39364

Pendleton P, Wu SH, Badalyan A (2002) Activated carbon oxygen content influence on water and surfactant adsorption. J Colloid Interface Sci 246(2):235–240. https://doi.org/10.1006/jcis.2001.8052

Pereira MFR, Soares SF, Órfão JJM et al (2003) Adsorption of dyes on activated carbons: influence of surface chemical groups. Carbon 41(4):811–821. https://doi.org/10.1016/S0008-6223(02)00406-2

Piai L, Dykstra JE, Adishakti MG et al (2019) Diffusion of hydrophilic organic micropollutants in granular activated carbon with different pore sizes. Water Res 162:518–527. https://doi.org/10.1016/j.watres.2019.06.012

Radovic LR, Silva IF, Ume JI et al (1997) An experimental and theoretical study of the adsorption of aromatics possessing electron-withdrawing and electron-donating functional groups by chemically modified activated carbons. Carbon 35(9):1339–1348. https://doi.org/10.1016/S0008-6223(97)00072-9

Rivera-Utrilla J, Bautista-Toledo I, Ferro-García MA et al (2001) Activated carbon surface modifications by adsorption of bacteria and their effect on aqueous lead adsorption. J Chem Technol Biotechnol 76(12):1209–1215. https://doi.org/10.1002/jctb.506

Rivin D (1971) Surface properties of carbon. Rubber Chem Technol 44(2):307–343. https://doi.org/10.5254/1.3547370

Rizzo L, Malato S, Antakyali D et al (2019) Consolidated vs new advanced treatment methods for the removal of contaminants of emerging concern from urban wastewater. Sci Total Environ 655:986–1008. https://doi.org/10.1016/j.scitotenv.2018.11.265

Saal L, Dittmann D (2021) TGA-FTIR-hyphenation-tool-kit. BAMResearch. https://doi.org/10.5281/zenodo.4917313

Speight JG (2015) Proximate analysis. In: Handbook of coal analysis. John Wiley & Sons, Ltd, pp 116–143, https://doi.org/10.1002/9781119037699.ch5

Suhas Carrott PJM, Ribeiro Carrott MML (2007) Lignin – from natural adsorbent to activated carbon: a review. Bioresour Technol 98(12):2301–2312. https://doi.org/10.1016/j.biortech.2006.08.008

Tagliavini M, Weidler PG, Njel C et al (2020) Polymer-based spherical activated carbon – ultrafiltration (UF-PBSAC) for the adsorption of steroid hormones from water: Material characteristics and process configuration. Water Res 185(116):249. https://doi.org/10.1016/j.watres.2020.116249

Thommes M, Kaneko K, Neimark AV et al (2015) Physisorption of gases, with special reference to the evaluation of surface area and pore size distribution (IUPAC Technical Report). Pure Appl Chem 87(9–10):1051–1069. https://doi.org/10.1515/pac-2014-1117

Várhegyi G, Antal MJ, Jakab E et al (1997) Kinetic modeling of biomass pyrolysis. J Anal Appl Pyrolysis 42(1):73–87. https://doi.org/10.1016/S0165-2370(96)00971-0

Viegas RMC, Mestre AS, Mesquita E et al (2020) Assessing the applicability of a new carob waste-derived powdered activated carbon to control pharmaceutical compounds in wastewater treatment. Sci Total Environ 743(140):791. https://doi.org/10.1016/j.scitotenv.2020.140791

Worch E (2021) Adsorption technology in water treatment. De Gruyter. https://doi.org/10.1515/9783110715507-202

Zietzschmann F, Aschermann G, Jekel M (2016) Comparing and modeling organic micro-pollutant adsorption onto powdered activated carbon in different drinking waters and WWTP effluents. Water Res 102:190–201. https://doi.org/10.1016/j.watres.2016.06.041

Zietzschmann F, Stützer C, Jekel M (2016) Granular activated carbon adsorption of organic micro-pollutants in drinking water and treated wastewater – aligning breakthrough curves and capacities. Water Res 92:180–187. https://doi.org/10.1016/j.watres.2016.01.056